On the evolution of the Solar Photospheric and Coronal Magnetic Field

Brian N. Handy

Department of Physics, Montana State University – Bozeman,

P.O. Box 173840, Bozeman, MT 59717

and

Carolus J. Schrijver

Stanford-Lockheed Institute for Space Research,

O/L9-41, B-252, 3251 Hanover Street, Palo Alto, CA, 94304

Received ______________________; accepted ______________________

August 3, 2000

ABSTRACT

The *Extreme-ultraviolet Imaging Telescope* (EIT) and the *Michelsen Doppler Imager* (MDI) instruments on the *Solar & Heliospheric Observatory* (SOHO) ran a coordinated observing campaign over the dates August 10–14, 1997. MDI generated 1.2 arc sec resolution magnetograms (0.6 arc sec pixels) of the solar photosphere at a nominal cadence of one minute, while EIT observed Fe XII (195 Å) (5 arc sec resolution; 2.5 arc sec pixels) in the MDI high-resolution field of view at a cadence of $\sim$17 minutes. We investigate the relationship between the quiet sun photospheric magnetic field and the quiet solar corona by first removing instrumental effects from the EIT data, time-averaging the MDI data for improved statistics, and coaligning the two datasets and applying solar rotation tracking. At the time of the observation, this was the longest continuous run of its kind. We conduct a detailed investigation of the processes of evolution in the photospheric magnetic field and look for sympathetic effects in the solar corona. We measure the lifetimes, dimensions and orientations of small-scale coronal brightenings and reconcile these processes against the evolution of the underlying photospheric magnetic field. Using statistics collected from this study we find that emerging bipoles in quiet sun reach a typical length of ≈ 14 Mm before fading or reconnecting to other flux concentrations in a time period of $\approx 5 - 12$ hours, and the quiet solar corona completely decorrelates in approximately 15 hours. We find that the majority large coronal loops in quiet sun are the product of numerous smaller magnetic flux concentrations coalescing in the photosphere rather than the product of a single large emerging bipole. This continuous process of emergence and coalescence leads to the observation that there is no prefered orientation to small-scale coronal brightenings in the solar corona.

August 3, 2000

1. Introduction

Observations of the quiet solar corona have advanced steadily over the years, primarily beginning with the first observations of the corona with the *Skylab* S-054 X-ray telescope (Vaiana et al. 1970), the X-Ray Polychromator (Acton et al. 1980), the *Yohkoh*/SXT telescope (Tsuneta et al. 1991), the SOHO/EIT instrument (Delaboudinière et al. 1995), and recently the *TRACE* observatory (Handy et al. 1999).

The *Solar & Heliospheric Observatory* (SOHO, Domingo et al. 1995) provided the first opportunity to simultaneously observe the solar photosphere and corona at a high temporal cadence, unhindered by atmospheric seeing, spacecraft night, or the Earth's radiation belts over an extended period of time. In particular it is interesting to compare the evolution of the photospheric magnetic field as seen by the Michelsen Doppler Imager (MDI, Scherrer et al. 1995) to that of the solar corona observed by the Extreme-Ultraviolet Imaging Telescope (EIT, Delaboudinière et al. 1995). Long-duration studies of the Sun's magnetic field have shown that the photospheric magnetic field is continually evolving on all size scales, at the finest time resolutions currently available. To put this in perspective, it has been found that in quiet Sun, as much flux is canceled as is present in these regions every 1.5–3 days (Schrijver et al. 1997). This implies a similar level of activity in the solar corona. SOHO's continuous view of the Sun has also made it possible to make long-duration observations of the relationship between the photospheric magnetic field and the quiet solar corona (Schrijver et al. 1998). Schrijver et al. studied data from a joint EIT Fe XII (195 Å) and MDI magnetogram observation that spanned a period of 106 hours. This study was limited in that the cadence of the EIT images was of the order of 30 minutes, and the authors of that study found the changes in quiet Sun morphology between images was quite significant.

In this paper we present an analysis of a sequence of joint EIT Fe XII (λ 195 Å)

August 3, 2000

observations of the ∼1.6 MK solar corona and MDI photospheric longitudinal magnetograms of the quiet Sun near disk center. For a period of 85 hours MDI obtained one magnetogram per minute its high-resolution field of view and EIT concurrently imaged the solar corona at a cadence of ≈16 minutes for the duration of the campaign (section 2). This campaign provided EIT images at a cadence approximately 30% faster than that of Schrijver et al. (1998). While the campaign is for a shorter period of time, we find that the duration of the campaign was adequate to observe the complete lifetimes of features near the resolution limit of EIT in quiet Sun.

We consider the evolution of the quiet solar corona in response to the activity of the photospheric magnetic field over the duration of the campaign. An understanding of the physical relationship between the evolution of the underlying photospheric magnetic field and structures in the corona is one requirement for understanding the processes responsible for driving the formation and evolution of coronal brightenings. We describe the qualitative evolution of the corona in response to the motions of the photospheric flux concentrations, we look for corresponding length scales in the photospheric magnetic field and the solar corona. We measure the characteristic lifetime of the quiet solar corona and compare these results to the lifetimes of magnetic phenomena as presented in Schrijver et al. (1998).

2. Observations

A special observing campaign was performed by EIT and MDI for a period of 85 hours from 10-Aug-1997 14:00 UT to 14-Aug-1997 03:00 UT. MDI high-resolution magnetograms were collected once per minute with occasional interruptions for full-disk magnetograms every 96 minutes, antenna handovers and other irregular, less frequent circumstances. The longest break in MDI magnetogram data over the course of the campaign spans three hours. EIT observed in the Fe XII channel (195 Å) with a temporal cadence of ≈ 17 minutes.

August 3, 2000

Periodic interruptions for the EIT synoptic program and other events are generally no more than one hour in duration.

The MDI field of view selected for this campaign spanned a region of 620×387 arcsec centered on the central meridian, ranging from latitudes of north. 40 arc seconds north of disk center to 430 arc seconds north. The EIT field of view was 256×256 pixels (660×660 arc seconds), containing the MDI field of view (figure 1).

August 3, 2000

3. Data Preparation

The raw MDI images were coaligned and averaged over 7 minute intervals centered on the EIT observation times and rebinned to 1.2 arc second pixels. Conversion factors from the FITS headers (BSCALE and BZERO), which trace back to instrument calibration, were used to convert raw data numbers to physical units. The conversion used was $B = 1.232 + 2.816(\mathrm{DN})$ where DN (*data numbers*) is the raw value from the FITS data file and B is the equivalent field strength $B = \Phi/A$, in units of Gauss (Scherrer et al. 1995, also Tarbell, T. D., private comm.). The EIT Fe XII data were degridded, flat fielded, dark current subtracted, normalized to a 1 second exposure rate and interpolated to 1.2 arcsec pixels with the IDL *SolarSoft* package (Freeland & Handy 1998). The EIT data were prepared with calibration data from 10-Nov-1997. Both datasets were subsequently coaligned via the pointing information in the FITS header, and further refined by visual inspection. The dataset was corrected for rigid solar rotation for further analysis.

The Fe XII quiet Sun regions in Figure 1 show in particular two elements of the solar corona: a pattern of compact, rapidly varying coronal brightenings and also a large-scale diffuse haze. This haze is a diffuse component of the solar emission which we are unable to associate with any specific magnetic features in the photospheric magnetograms. Schrijver

& McMullen (2000) have associated this haze with resonant scattering in the solar corona. In order to increase the contrast of the small-scale structures this diffuse haze was reduced via a spatial high-pass filter (c.f. figure 3). The filtered images are displayed with a linear scale and when compared to the flux concentrations in the photospheric magnetograms, small-scale coronal connectivity is much more evident. A side effect of this process is the geometry of large-scale loops will be affected: small, compact structures ($\lesssim 5$ arcsec) will emerge from the process very similar in size and shape to the initial images, but the geometry of larger structures near the characteristic size of the filter (typically long structures with widths $\gtrsim 5$ arcsec) are subject to some distortion: large uniform structures may be filtered out entirely. Noise and image artifacts are also enhanced—although the EIT grids and CCD flatfield have been removed from the images prior to filtering, vestiges of them remain and are amplified by this process.

4. Flux Emergence and Coronal Brightenings

We find in general all flux emergences and cancellations above a threshold of 10^{18} Mx were associated with a noticeable brightening in the Fe XII corona. In contrast, fewer than 25% of all emerging bipoles may be expected to appear as a brightening in images from the *Yohkoh*/SXT (Harvey 1997). The higher quantity of loop brightenings visible in the fe XII images relative to the corresponding images from the SXT instrument is partially an issue of physics, partially one of sensitivity. Brosius et al. (1996) evaluated the differential emission measure (DEM) distribution for several quiet and active sun regions and found that, in the case of quiet sun, the peak DEM occurred at a temperature of $\approx 1.2 \times 10^6$ K, and essentially dissappeared above 4×10^6 K: the quiet sun is comparatively cool, relative to active regions. The Fe XII channel of EIT has its greatest sensitivity at a temperature of $\approx 1.6 \times 10^6$ K — very near this peak — while the sensitivity of the AlMg channel of

August 3, 2000

the SXT instrument is most sensitive to plasma temperatures of $\gtrsim 3.0 \times 10^6$ K (Tsuneta et al. 1991; Delaboudinière et al. 1995). At 1.6×10^6 K, the EIT/195 Å channel sensitivity is approximately 10× greater than that of the SXT AlMg channel. The small component of high-temperature plasma to be found in quiet sun will not be visible above the instrumental noise in the SXT instrument.

Our observations confirm this analysis. On the smallest spatial scales and at the lowest intensities, we observe these loops often have no counterpart in the more energetic SXT images. Emerging loop structures first become visible in the corona when the flux tube separation reached 4.5–8.5 Mm and remained visible for typically 5–12 hours after the initial brightening before fading or reconnecting to other preexisting flux concentrations. ("Fading loops" does not imply anything about the fate of the disappearing loops; we are simply unable to discuss those loops we can no longer see.) These reconnections are generally manifested as a gradual shift in brightness between the initial pair of footpoints and a new connection to the preexisting concentrations. Occasionally a glowing loop of plasma may be observed to shift from the old connection to the new connection. These expanding loop systems reached a maximum footpoint separation of about 14 Mm (figure 4). At this distance, the photospheric flux concentrations at the footpoints tend to merge with other flux concentrations. In the case of merging same-polarity flux concentrations,the coronal counterpart to these footpoints would subsequently reconnect to yet more distant concentrations. Emerging concentrations were not observed to expand to significantly greater distances via this mechanism. In many cases emerging flux pairs had reconnected to neighboring pre-existing flux concentrations before separating enough for the connecting loop to reach sufficient height to emit at coronal temperatures.

Emerging (canceling) regions in the movie were followed to their maximum separation forward (backward) in time. A survey of this maximum footpoint separation seen in the

August 3, 2000

EIT/MDI movie is shown in figure 4. The number of observations was limited by the size of the instrumental field of view and the total time of observation. In many cases it was not possible to observe the evolution of loop structures for the lifetime of the loop, as the loop structures were formed prior to the beginning of the observation, lasted past the end of the observation, or drifted out of the field of view. The most frequent maximum length was $\approx$ 14 Mm, slightly less than the average supergranule diameter of 15–18 Mm (Hagenaar et al. 1997). The average maximum length was $\approx$ 18 Mm.

Canceling magnetic flux tended to connect at an average footpoint separation of 14 Mm before converging and disappearing from the coronal images. Loops connecting canceling features disappeared from the EIT images at a separation of 4–7 Mm. Cases were noted where the opposing flux concentrations at the loop footpoints appeared to be in contact before the loop disappeared from the Fe XII channel, but the centroids of the magnetic footpoints were still separated by $\geq$ 4 Mm. This minimum separation arises from the requirement that the magnetic footpoints must separate sufficiently before the loops reach coronal heights and hence coronal temperatures. If we assume the loops are approximately semicircular in shape, this observation suggests the loops must reach a height of $\sim$ 3 Mm before appearing in Fe XII.

Emerging and canceling flux concentrations tend to only remain (or become) connected while at a distance equal to or shorter than about one supergranule diameter, $\approx$ 16 Mm (Hagenaar et al. 1997). When emerging flux pairs reach separation distances of this magnitude, they typically either cancel with other opposing flux concentrations or merge with same-polarity concentrations, following which they often reconnect to yet more distant opposite-polarity concentrations of similar strengths. In one particular case, a collection of emerging concentrations drifted along supergranular boundaries until the positive flux concentrations began to collect in a small region. The initial ensemble of positive

August 3, 2000

flux concentrations were initially spread over ≈ 30 Mm and were connected to points approximately 20 Mm distant. As the positive flux concentrations began to merge, they reconnected several times to a number of negative flux concentrations over the course of 30 hours. They subsequently coalesced into one flux element ≈ 14 Mm in diameter and reconnected to the negative pole of a large active region 110 Mm distant (figure 5). (This particular extreme example is not included in Figure 4 as one footpoint connected to one of the large active regions, out of the scope of that analysis.) The total absolute value of the magnetic flux at the isolated east pole of this loop at reconnection was $\approx 2 \times 10^{20}$ Mx, two orders of magnitude greater than typical quiet Sun flux concentrations (Schrijver et al. 1997). This reconnection can be seen to have a distinct effect on the magnetic configuration of the active region, even though the separation is so great that the active region is nearly out of the field of view by the time of reconnection. This particular example is an extreme version of a phenomenon often seen in this dataset on smaller spatial scales.

In one case, a flux concentration was observed to be connected to a distant concentration while simultaneously canceling against a neighboring opposite polarity bundle. No loop structure connecting these two canceling polarities was evident in the Fe XII images, as the temperature of any connecting loops was probably below the bandpass of the Fe XII channel, in agreement with the ≥ 4 Mm limit mentioned earlier.

We observed several phenomena germane to both emerging and canceling flux. There were numerous cases in which the coronal brightening connecting two footpoints favored the footpoint containing the largest amount of flux, in that the brightening was most obvious over the larger footpoint. In our filtered images the loops often appeared to taper in diameter from one flux concentration to the other instead of forming a loop of constant diameter. Studies from an observatory such as TRACE show that many of the monolithic loops we discuss in this paper are resolved as a conglomerate of finer-scale coronal threads

August 3, 2000

when seen at the higher resolution (Schrijver et al. 1999).

The variation in intensity from the coronal loops was observed to vary rapidly in comparison with the change in the anchoring magnetic flux concentrations. Harvey et al. (1994) suggest that the variability of bright points has little to do with the rate of magnetic flux change in the underlying magnetic structure but instead has to do with the relative motion of those structures. Coronal loop structures are also observed to deform and stretch in response to the evolution of the neighboring unconnected magnetic field. The observed motion is dependent on the flux strength and proximity of the neighboring field, and connection to that is further dependent on any apparent connections that flux concentration has elsewhere. This motion appears to happen over time rather than an instantaneous accommodating response to changes in neighboring flux concentrations. Rather, it evolves in a smooth manner at a pace consistent with the rate of evolution and strength of the neighboring field.

Emerging flux pairs were never observed to expand to distances in excess of about one supergranule diameter, but the mere existence of many loops in various stages of development on length scales greater than this distance all over the quiet Sun suggests this discontinuous stepwise process of emergence, coalescence and reconnection is in a constant state of motion. When a sufficient quantity of flux concentrations coalesce, the coronal magnetic field tends to restructure to adapt to these new boundary conditions. We found that as magnetic flux concentrations coalesced into larger concentrations, they always tended to reconnect to other similarly coalescing flux concentrations.

August 3, 2000

5. Length Scales in the Corona

We now generalize beyond emerging and canceling phenomena and consider all quiet Sun brightenings visible in the Fe XII channel during this campaign. In section 4 we described the existence of several domains of loop sizes present in the quiet corona. Loops that are larger than the average supergranule diameter are typically the product of merging flux concentrations at the photospheric level and corresponding reorganization of the coronal magnetic field. A histogram of footpoint separation associated with coronal loops is shown in figure 6. These statistics were collected by measuring the footpoint separation for all coronal loops that could be clearly associated with opposite polarity footpoints from three quiet Sun regions over the duration of this observing campaign.

This figure shows a histogram with a most frequently occurring length of ≈ 12 Mm and an average of 18 Mm. There is a cutoff at 3.8 Mm (2.59 arcsec) at the limiting resolution of EIT full-resolution pixels, though features smaller than this have been seen by TRACE (Golub et al. 1999; Schrijver et al. 1999). Quiet region loops with footpoint separations $\gtrsim 35$ Mm are generally dimmer and more difficult to see against the diffuse background (Rosner et al. 1978; Klimchuk 1992). Loop structures were excluded from this distribution if it was not possible to unambiguously associate a pair of opposite-polarity footpoints with the coronal brightening. Several examples of coronal structures that lacked an obvious connection to an opposite-polarity footpoint elsewhere were not include in this sample. This included many brightenings that originated at one footpoint and disappeared into the background, or connected to flux concentrations somewhere outside of the field of view.

This distribution of loop lengths (or, more specifically, photospheric footpoint separations) may be modeled analytically. If one assumes a random distribution of magnetic flux concentrations of one polarity and then places a flux element of the opposite polarity in this field, then the probability distribution $\mathcal{P}(r)$ describing the distance to the nearest

August 3, 2000

neighbor is given by Kendall & Moran (1963)

$$\mathcal{P}(r)dr = 2\lambda\pi r e^{-\lambda\pi r^2} dr \tag{1}$$

where r is the radial distance and λ is the density of points on the plane ($\lambda = 1/S$; S has units of area). This function was fit to the distribution with λ as the free parameter and the χ^2 test was used to evaluate the goodness of fit.

The best fit (lowest χ^2) was given by $S = 1/\lambda = 1260$ Mm^2. This analytical fit was tested against the measured distribution and the results were compared via the *Kolmogorov-Smirnov* (K-S) statistical test (Press et al. 1992). The confidence level of equation 1 to the data found by the K-S test is found to be 0.159, consistent with the null hypothesis.

The relatively low significance is related in part to the assumptions that eq. 1 imposes. This relation assumes that all coronal loops will form connections between nearest neighbors, but careful studies of the merged EIT/MDI movie created for this work shows this not always to be the case. This relation also assumes that the flux concentrations are distributed randomly on the photosphere, but flux concentrations tend to accumulate in the granular and supergranular boundaries, giving rise to a more ordered motion than that of a random walk (CITE, e.g. some A.M.Title photospheric granular paper here).

The area S encloses a *pair* of opposite polarity flux concentrations, so the area per flux concentration is half of this value or 630 Mm^2. Measurements of the distribution of cell sizes in the Ca II chromospheric network show a mean area of ≈ 610 Mm^2 (Hagenaar et al. 1997), in close agreement with our observation. Hagenaar et al. (1997) measured the geometry of the chromospheric network, ignoring the structure and location of the magnetic flux concentrations. The values derived from Fig. 6 include a bias arising from some connections between flux concentrations that don't obey the nearest-neighbor concept. This would have a tendency to slightly increase the average loop footpoint separation, as is demonstrated by

August 3, 2000

our result.

Schrijver et al. (1997) measured the number density of flux concentrations in quiet network. Their study showed that histograms of the frequency of flux concentrations with a given core flux content could be modeled by an exponential over the range 1–5$\times 10^{18}$, e.g.

$$n = n_0 \exp\left(-\frac{\Phi}{\Phi_0}\right) \tag{2}$$

where n_0 and Φ_0 are constants, Φ is the threshold flux level and n is the number density of photospheric flux concentrations. The slope of the exponential $\Phi_0 \approx 3 \times 10^{18}$ Mx, which then implies the average total flux per concentration was found to be $\langle\Phi\rangle = \Phi_0 \approx 3 \times 10^{18}$ Mx (assuming the fit in eq. 2 extends over the entire range). The footpoint separation (from the MDI magnetograms) was correlated to the flux intensity in the footpoints (figure 7), using the filtered Fe XII images to show connectivity between the footpoints. The centroids of the footpoints were used to determine the separation, and the flux intensity was calculated as the integral of the flux over an area described by the ± 25 gauss contours of the footpoints in the magnetograms. Presumably the flux in the loop is no greater than that in the weakest polarity footpoint, so the footpoint with the least amount of flux was used in this correlation. There is significant scatter in the correlation, but a few observations are evident. First, it is apparent that in order to see a brightening in the EIT Fe XII images, the flux in the loop must satisfy $|\Phi| \gtrsim 3 \times 10^{18}$ gauss. It is also evident that for large values of footpoint separation, a correspondingly larger magnetic flux is required to maintain the loop connectivity (the minimum value approaches 10^{19} Mx for separations $\gtrsim 40$ Mm). Similarly, there is also a second trend for large flux concentrations to connect at greater distances. When existing flux concentrations merge and form larger concentrations, they are then free to reconnect to flux concentrations of similar strength over a wider range of distances, ranging from immediate neighbors (at distances of $\lesssim 10$ Mm) to far-reaching concentrations at distances of > 55 Mm. The strongest footpoints can be noted to connect

August 3, 2000

to opposite polarity footpoints at any distance shown in the figure.

Hagenaar (1998, private communication) calculated the relationship between threshold flux levels and the resulting separation of flux concentrations based on the quiet Sun data used elsewhere in this paper (figure 8). The MDI data was smoothed with a 1.2 arc second Gaussian, then flux concentrations that exceeded the two-σ noise level (14 gauss) were selected for analysis. The density of points was calculated based on only counting those flux concentrations of magnitude greater than the threshold flux level. Based on the average cell diameter of 18 Mm from figure 6, this figure predicts a minimum footpoint flux concentration of $\approx 2 \times 10^{18}$ Mx in the loop. This is comparable to the minimum flux concentration of $\approx 3.5 \times 10^{18}$ Mx in figure 7.

Another technique for evaluating the relationship between loop footpoint separation and magnetic flux intensity is to integrate all unsigned flux in the region of the coronal brightening. Schrijver et al. (1998) calculated the flux as all flux above the two-σ noise level ($\sigma = 7$ gauss) in a circle of diameter 27 Mm, under the assumption that the loop is affected by *all* flux in nearby proximity to the coronal brightening. This assumption is bolstered by the results of Fisher et al. (1998), who correlated global properties of vector magnetograms from the University of Hawaii's Mees Solar Observatory and found a very good correlation between X-ray luminosity over the entire active region and the total unsigned magnetic flux $\Phi_{tot} \equiv \int dA|B_z|$. In figure 9 we integrate over the area bounded by the loop brightening visible in the filtered Fe XII images and the coronal loop footpoints evident in MDI and see a similar correlation between these two quantities. This study is concerned with flux concentrations and loop sizes much smaller than the active regions discussed in Fisher et al. (1998), but we reach a similar conclusion regarding the correlation between footpoint separation and $|B_z|$.

In figure 10 we compare the total unsigned flux under the loop to the total integrated

August 3, 2000

intensity of the loop in Fe XII. This agrees with the analytical work of Fisher et al. (1998) and the theoretical predictions of Longcope (1996), who predicts a qualitative variation of the luminosity with Φ_{tot}. This correlation is quite linear and is an extension to the analysis of Schrijver (1990) who suggested a power law fit of $L \sim \Phi_{tot}^{1.0}$ for a 1 MK corona for large-scale magnetic fields.

August 3, 2000

6. Autocorrelation

Whereas the previous method of measuring the size and separation of coronal loops was done manually, e.g. measured by hand directly from the data, it is biased by the ability of the observer to see the connections and accurately measure the distances involved. An alternative method that removes part of this bias at the expense of adding new ones is to perform an autocorrelation analysis of the EIT images. This method favors the large-scale structures in the images, so the bias in the measurement of coronal loop structures is that the final result will be weighted towards the larger structures. The correlation analysis that follows was limited to quiet Sun regions to reduce this bias.

In figure 11 we show typical autocorrelation amplitudes in the linearly-scaled EIT Fe XII movie. Three quiet regions were chosen from the full field of view of the observation in an effort to mitigate effects from the large-scale loops connecting the two active regions. The autocorrelation curve was calculated from the linearly-scaled images over a lag of ± 60 Mm for each frame in the field of view. This array of correlations was then averaged to yield the curves in figure 11. The anisotropy in N-S and E-W correlation in the eastern and central regions indicates these regions were affected by the presence of overlying loops, which were faint but apparent in the prepared movie. The western region was free of this effect, and the correlation plot for this region suggests that quiet Sun coronal brightenings are generally isotropic in their orientation.

The *a priori* assumption was that the loops would be biased towards an east-west orientation as is typical of large active regions. However, aside from the influence of the large-scale active region loops, the autocorrelation curves show little difference in the N-S and E-W directions. We would expect to see some consistent anisotropy in the two directions, an indication of correlating along the length of the loop in the E-W direction and across the narrower width of the loop in the N-S orientation. The present result is in qualitative agreement with inspection of the data by eye: *there is no preferred orientation of small-scale coronal loops.*

This isotropy in loop orientation is to be expected, however. We note that the size of the magnetic flux concentrations found at the footpoints of the loops in this study are quite small, often on the order of 10^{18} Mx. As one progresses towards smaller flux concentrations, the Hale Polarity Law (Hale 1919) seems to apply less cleanly. Harvey-Angle (1993, chapter 3) studied the orientation of emerging active regions and found that as the size of the region decreased, the orientation of the magnetic bipole beneath the region became less likely to align with a preferential rotation. These results are an extension of Harvey's study to smaller features and cooler temperatures. There are likely several phenomena in effect at these smaller sizes and domains. First, the smallest magnetic flux concentrations are more likely to be influenced by the motions of the Sun's convective layer and hence will be subject to significant mixing and shifting before reaching the photosphere. Once at the surface, the flux concentrations are subject to constant shifting and subsequent reconnection in the corona to other flux concentrations, discussed qualitatively in section 4. Any preferential orientation of flux concentrations at emergence will be rapidly dispersed as the concentrations reconnect to other, randomly-oriented neighboring flux concentrations.

With a grasp on the size of coronal features, it is then useful to consider the lifetimes of coronal loops via cross-correlation. We compare a series of images in time to the first

August 3, 2000

image and plot the cross-correlation amplitude as a function of time (figure 12). This study used the same regions as were used for the autocorrelation method discussed previously, and the time domain of the graphs runs for the length of time each field of view was fully present in the images. The lifetime of the structures visible in the corona is measured as the amount of time necessary for the cross-correlation amplitude to drop to a factor of $1/e$, at which point we consider the region to be completely decorrelated—having no "memory" of its previous structure. We find the quiet 1 MK corona has a timescale of nominally 14–20 hours.

7. Discussion

This work is a detailed analysis of the evolution of the quiet sun corona in response to motions of the photospheric magnetic field, based on an 84 hour coordinated observing campaign involving SOHO/EIT and MDI. The long duration and consistent, steady cadence (≈ 17 minutes for the EIT observations, with few interruptions) of this campaign was highly suitable for the study of the evolution and lifetime of small-scale coronal structures.

We find that the dimmest quiet Sun coronal brightenings tend to be hidden by a diffuse coronal haze present in the Fe XII images. When this haze (which varies slowly both spatially and temporally) is removed from the data with a spatial high-pass filter, the contrast of small-scale and other low-intensity loop structures is significantly enhanced. The resulting filtered images and movies show an amazingly high level of coronal connectivity between photospheric flux concentrations, a much higher fraction than that found by Harvey (1997) in soft X-ray images. We attribute this to the higher sensitivity of the EIT Fe XII channel to quiet sun regions as compared to the *Yohkoh*/SXT instrument.

From the high-pass filtered data we find that all photospheric flux concentrations

August 3 2000

$\gtrsim 3 \times 10^{18}$ Mx are associated with coronal brightenings visible in the EIT Fe XII (1.3 MK) channel. These observations are in near agreement with Schrijver et al. (1998), who found a similar threshold (using the same instrumentation). Based on this work, it is not clear if this is an intrinsic threshold (implying photospheric concentrations smaller than these do not tend to connect via loops sufficiently high in the atmosphere to reach coronal temperatures) or an instrumental threshold (arising from instrumental resolution and detector sensitivity). We also find that emerging flux in quiet Sun is never seen to expand to size scales we would associate with large-scale ($\gtrsim$ 15 Mm) coronal loops. (The converse statement — large scale loops never converge and cancel against their own footpoints — also applies.) What instead happens is a continuous process of discontinuous reconnection events: magnetic flux pairs emerge from the photosphere, migrate along the supergranular lanes, merge and/or cancel against other preexisting flux concentrations and the associated coronal loops adjust accordingly. As the amount of flux present in a particular photospheric concentration increases, that increased flux generally reconnects over a larger area to cover the matching amount of opposite polarity to satisfy $\nabla \cdot \mathbf{B} = 0$. of that connection grows, and we find the maximum footpoint separations accessible to a bipole grows with increasing flux (figure 7). These bipoles may either connect to opposite-polarity concentrations of similar or greater strengths, or may connect to several concentrations over a range of distances.

This last observation complicates other efforts at correlating the corona to events in the photosphere. Attempts to compare the typical scale size of coronal features (section 5) to the magnetic field are frustrated by this issue of coronal loop connectivity. By direct measurement from the images we find typical small-scale brightenings with an average length of 18 Mm and via correlation methods the size scale is found to be somewhat larger at ≈ 26 Mm. The former approach is biased towards smaller, brighter features while the latter approach is biased in favor of large, bright structures which may explain the variation in size scales. Autocorrelation reveals other interesting features of the quiet corona:

August 3, 2000

small-scale coronal loops in the quiet Sun are isotropic in their orientation. Small-scale flux concentrations (typically $\lesssim 2$ Mm in size) are strongly influenced by the motions of the solar convective zone, while the large active region flux concentrations that are seen to obey this law are more resistant to being shifted about. Perhaps even more likely is the concept that even if the emerging flux were to emerge with a favored polarity orientation, the coronal reconnection events that follow within hours of emergence will most likely significantly alter the orientation of the coronal brightening. Isotropy in coronal brightening orientation is a natural consequence of (1) the moving, merging and cancellation of magnetic flux concentrations, and (2) the isotropic nature of the quiet Sun photospheric magnetic field: concentrations uniformly separated by about the diameter of a supergranular cell will have little effect on the orientation of coronal loops once the process of reconnection to other magnetic sources begins.

The high resolution observations possible with the MDI instrument (0.6 arc second pixels or 870 km resolution) show significant structure at the level of instrumental resolution, and temporal evolution significantly faster than the 17 minute cadence of this campaign. Observations have been made since this work by the *Transition Region and Coronal Explorer* (Handy et al. 1999, TRACE,) show unresolved structures at the limiting resolution of that instrument (0.5 arc seconds or 725 km) (Schrijver et al. 1999), with significant structural changes obvious at cadence on the order of seconds. More recently, Wang et al. (2000) observed a C5.7 flare in H α with a spatial resolution of 0.6 arc seconds and a temporal resolution of 33 msec. Fluctuations in visible structures were apparent even at these resolutions.

We thank the EIT and MDI-SOI teams for their efforts in operating the instruments and also for their assistance with the data preparation and analysis. BNH is grateful to the Solar & Astrophysics Group at Lockheed-Martin, who accomodated him as a graduate

August 3, 2000

student during the preparation of this work. SOHO is a mission of international cooperation between ESA and NASA. This work was supported by NASA contract NAS5-38099 and NSF grant ATM953-1776.

August 3, 2000

REFERENCES

Acton, L. W., Culhane, J. L., Gabriel, A. H., Bentley, R. D., Bowles, J. A., Firth, J. G., Finch, M. L., Gilbreth, C. W., Guttridge, P., Hayes, R. W., Joki, E. G., Jones, B. B., Kent, B. J., Leibacher, J. W., Nobles, R. A., Patrick, T. J., Phillips, K. J. H., Rapley, C. G., Sheather, P. H., Sherman, J. C., Stark, J. P., Springer, L. A., Turner, R. F., & Wolfson, C. J. 1980, Sol. Phys., 65, 53

Brosius, J. W., Davila, J. M., Thomas, R. J., & Monsignori-Fossi, B. C. 1996, ApJS, 106, 143

Delaboudinière, J. P., Artzner, G. E., Brunaud, J., Gabriel, A. H., Hochedez, J. F., Millier, F., Song, X. Y., Au, B., Dere, K. P., Howard, R. A., Kreplin, R., Michels, D. J., Moses, J. D., Defise, J. M., Jamar, C., Rochus, P., Chauvineau, J. P., Marioge, J. P., Catura, R. C., Lemen, J. R., Shing, L., Stern, R. A., Gurman, J. B., Neupert, W. M., Maucherat, A., Clette, F., Cugnon, P., & Van Dessel, E. L. 1995, Sol. Phys., 162, 291

Domingo, V., Fleck, B., & Poland, A. I. 1995, Sol. Phys., 162, 1

Fisher, G. H., Longcope, D. W., Metcalf, T. R., & Pevtsov, A. A. 1998, ApJ, in press.

Freeland, S. L. & Handy, B. N. 1998, Sol. Phys., 182, 497

Golub, L., Bookbinder, J., DeLuca, E., Karovska, M., Warren, H., Schrijver, C. J., Shine, R., Tarbell, T., Title, A., Wolfson, J., Handy, B., & Kankelborg, C. 1999, Phys. Plasmas, 6, 2205

Hagenaar, H. J., Schrijver, C. J., & Title, A. M. 1997, ApJ, 481, 988+

Hale, G. E. 1919, ApJ, 49, 153+

August 3, 2000

Handy, B. N., Acton, L. W., Kankelborg, C. C., Wolfson, C. J., Akin, D. J., Bruner, M. E., Caravalho, R., Catura, R. C., Chevalier, R., Duncan, D. W., Edwards, C. G., Feinstein, C. N., Freeland, S. L., Friedlaender, F. M., Hoffmann, C. H., Hurlburt, N. E., Jurcevich, B. K., Katz, N. L., Kelly, G. A., Lemen, J. R., Levay, M., Lindgren, R. W., Mathur, D. P., Meyer, S. B., Morrison, S. J., Morrison, M. D., Nightingale, R. W., Pope, T. P., Rehse, R. A., Schrijver, C. J., Shine, R. A., Shing, L., Strong, K. T., Tarbell, T. D., Title, A. M., Torgerson, D. D., Golub, L., Bookbinder, J. A., Caldwell, D., Cheimets, P. N., Davis, W. N., DeLuca, E. E., McMullen, R. A., Warren, H. P., D., A., Fisher, R., Maldonado, H., & Parkinson, C. 1999, Sol. Phys., in press

Harvey, K. L. 1997, in ASP Conference Series, Vol. 111, Proc. of Observations of Magnetic Reconnection in the Solar Atmosphere, held in Bath, England, March 20-22, 1996, 9–18

Harvey, K. L., Strong, K. T., Nitta, N., & Tsuneta, S. 1994, in Solar active region evolution: Comparing models with observations, ed. K. S. Balasubramaniam & G. W. Simon (A.S.P.), 377–388

Harvey-Angle, K. L. 1993, PhD thesis, Sterrekundig Instituut, Universiteit Utrecht

Kendall, M. G. & Moran, P. A. P. 1963, Geometrical Probability, Griffin's Statistical Monographs & Courses No. 10 (Charles Griffin & Company Limited)

Klimchuk, J. A. 1992, in ESA, Proceedings of the First SOHO Workshop: Coronal Streamers, Coronal Loops, and Coronal and Solar Wind Composition, 167–176

Longcope, D. W. 1996, Sol. Phys., 169, 91

Press, W. H., Teukolsky, S. A., Vetterling, W. T., & Flannery, B. P. 1992, Numerical Recipes in FORTRAN, 2nd edn. (Cambridge University Press)

August 3, 2000

Rosner, R., Tucker, W. H., & Vaiana, G. S. 1978, ApJ, 220, 643

Scherrer, P. H., Bogart, R. S., Bush, R. I., Hoeksema, J. T., Kosovichev, A. G., Schou, J., Rosenberg, W., Springer, L., Tarbell, T. D., Title, A., Wolfson, C. J., Zayer, I., & The MDI Engineering Team. 1995, Sol. Phys., 162, 129

Schrijver, C. J. 1990, in Mechanisms of Chromospheric and Coronal Heating — Proceedings of the International Conference, Heidelberg, 5-8 June 1990, ed. P. Ulmschneider, E. R. Priest, & R. Rosner (Springer-Verlag), 257–272

Schrijver, C. J. & McMullen, R. A. 2000, ApJ, 531, 1121

Schrijver, C. J., Shine, R. A., Hurlburt, N. E., Tarbell, T. D., & Lemen, J. R. 1998, in Proceedings of the Fifth SoHO Workshop — The Corona and Solar Wind near Minimum Activity 17-20 June 1997, 669–674

Schrijver, C. J., Title, A. M., Berger, T. E., Fletcher, L., Hurlburt, N. E., Nightingale, R. W., Shine, R. A., Tarbell, T. D., Wolfson, C. J., Golub, L., Bookbinder, J. A., DeLuca, E. E., McMullen, R. A., Warren, H. P., Kankelborg, C. C., Handy, B. N., & De Pontieu, B. 1999, Sol. Phys., in press.

Schrijver, C. J., Title, A. M., Van Ballegooijen, A. A., Hagenaar, H. J., & Shine, R. A. 1997, ApJ, 487, 424+

Tsuneta, S., Acton, L., Bruner, M., Lemen, J., Brown, W., Carvalho, R., Catura, R., Freeland, S., Jurcevich, B., Morrison, M., Ogawara, Y., Hirayama, T., & Owens, J. 1991, Sol. Phys., 136, 37+

Vaiana, G. S., Krieger, A. S., Speybroeck, L. P., & Zehnpfennig, T. 1970, Bull. Am. Phys. Soc., 15, 611

August 3, 2000

Wang, H., Qiu, J., Denker, C., Spirock, T. J., Chen, H., & Goode, P. R. 2000, in AAS/Solar Physics Division Meeting, Vol. 32, 1406+

August 3, 2000

This manuscript was prepared with the AAS LATEX macros v5.0.

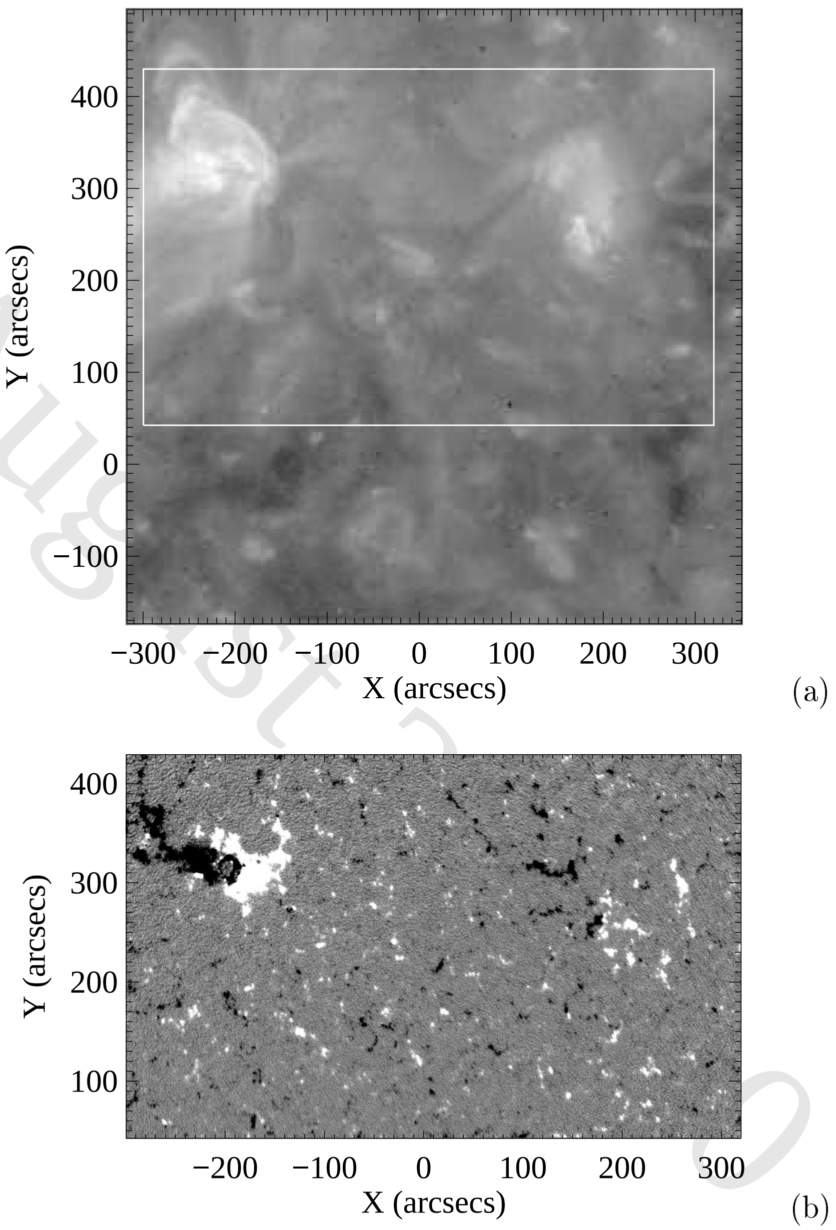

Fig. 1.— The EIT and MDI fields of view during the coordinated EIT/MDI observing campaign. Image (a) is the EIT Fe XII λ 195 Å field of view, displayed as log intensity. The EIT field of view was 256×256 full-resolution pixels (11×11 arc minutes). An outline of the MDI field of view is shown on the image. The time of observation is 12-AUG-1997 12:58:44 UT. Image (b) is the corresponding MDI high-resolution field of view of the

photospheric magnetic field, averaged over 7 frames centered around the EIT frame and scaled to ±50 Gauss. The MDI field of view was 1024×640 high-resolution MDI pixels (0.6 arc seconds/pixel, 10.3×6.5 arc minutes). The coordinates correspond to arc seconds from Sun center. North is up, west is to the right.

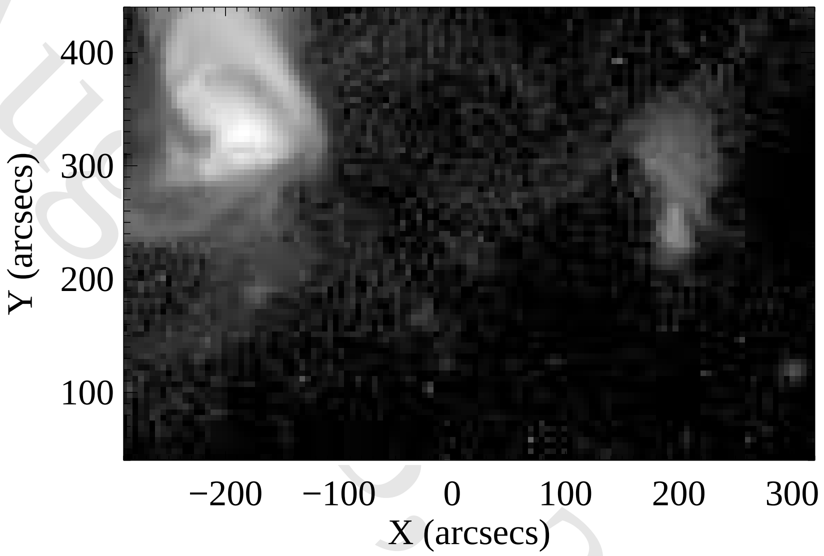

Fig. 2.— A *Yohkoh*/SXT image cotemporaneous with Figure 1. The time of observation is 12-Aug-97 14:01:22. This is a composite image of short+long exposures taken in the AlMg channel to increase the dynamic range.. Image resolution is 10.0 arc sec. The haze present in Figure 1 is not evident here, and the myriad of small-scale features present in the Fe XII data are also not evident in significant detail. The single bright (and dark) pixels are uncorrected hot CCD pixels.

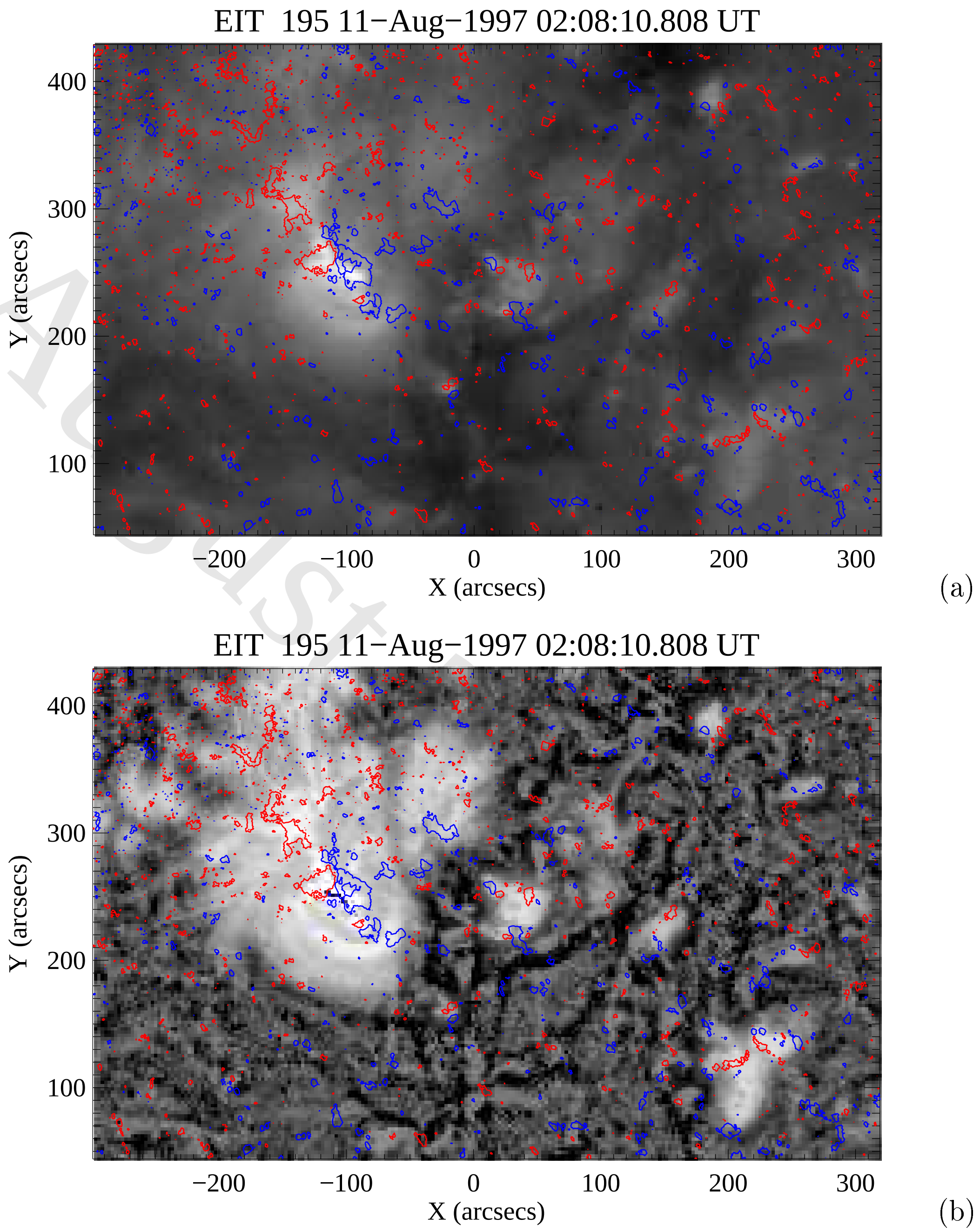

Fig. 3.— A comparison of a log-scaled EIT/Fe XII image to its high-pass filtered counterpart. (a) is the original EIT image displayed on a logarithmic scale. Image (b) is the same image, filtered to remove a diffuse overlying haze and increase the contrast of small dim coronal

loops. The contours represent the MDI photospheric magnetic field levels at ±25 Gauss.

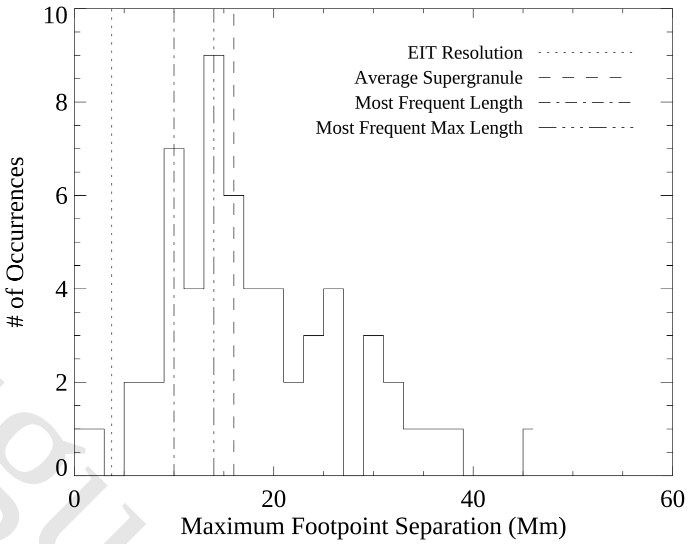

Fig. 4.— Maximum footpoint separations seen for emerging and canceling flux and their coronal loop counterparts in quiet Sun. Also indicated on the histogram is the limiting resolution of the EIT instrument, the most occurring length of footpoint separations from figure 6 and the average supergranule diameter from Hagenaar et al. (1997). The data point that falls below EIT resolution is a result of the loops blooming in the corona over a projected area larger than that of the photospheric footpoints.

August 3, 2000

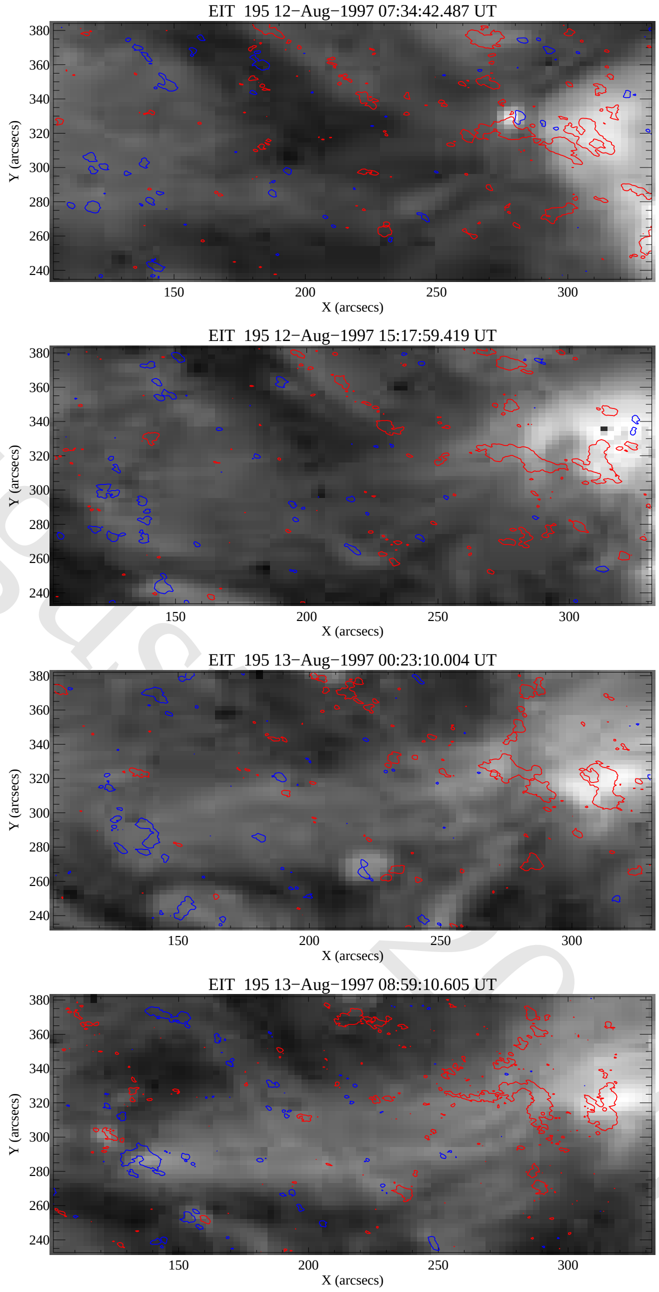

Fig. 5.— An illustration of flux collection and resultant magnetic reconnection in the corona. The positive flux concentration (left side of image, bottom frame) is about 14 Mm in diameter and has a total flux content of $\approx 2 \times 10^{20}$ Mx. The field of view is 450×280 Mm. The thin brightening drifting through the image (at center of bottom image, ≈ 25 degrees from

vertical) is an artifact of the CCD flat-field. The EIT image is log-scaled; MDI contours are ±25 gauss.

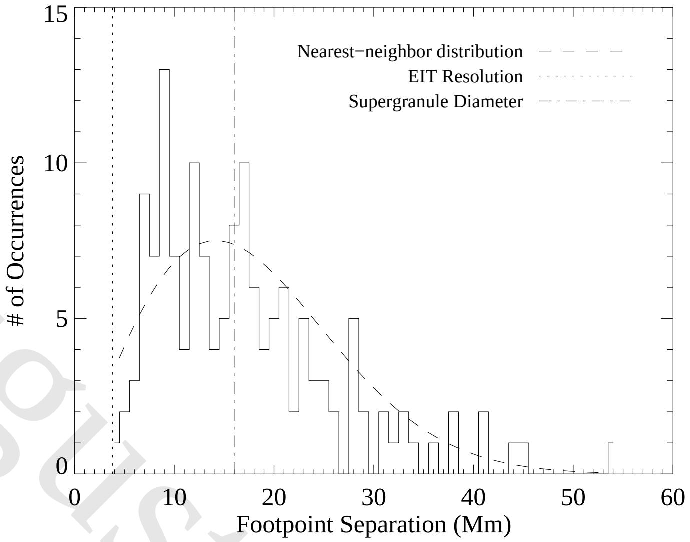

Fig. 6.— Distribution of coronal loop footpoint separations for loops visible in the EIT Fe XII (195 Å) Channel. The limiting resolution of EIT is 3.8 Mm and the average supergranule diameter (from Hagenaar et al. 1997) is ≈ 16 Mm. The dashed line represents the analytic nearest-neighbor probability distribution for bipole cell sizes (e.g. one positive – negative flux pair per cell) of 1260 Mm^2. The most occurring value of the distribution is ≈ 12 Mm, and the average value of this distribution is 18 Mm.

August 3, 2000

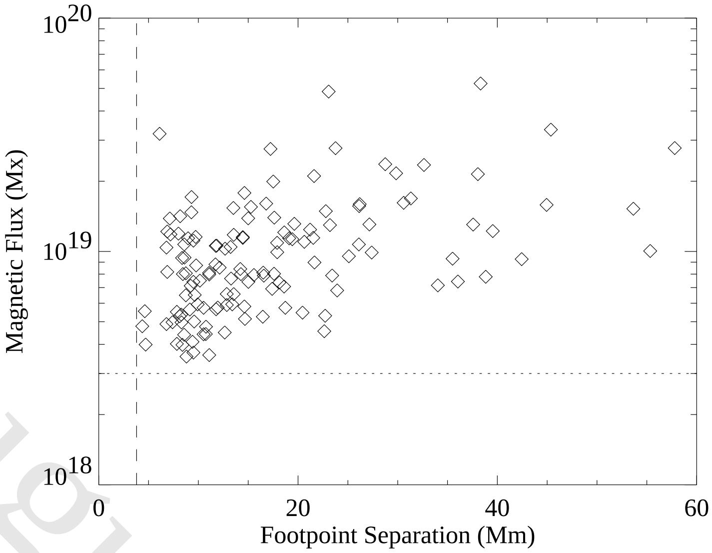

Fig. 7.— The footpoint separation of coronal brightenings in EIT Fe XII vs. the magnetic flux concentration in one footpoint. The flux was found by integrating the flux over an area defined by the ±25 gauss contour lines, and the flux from the smaller of the two concentrations was used for this figure. The dotted line is the average flux concentration found by Schrijver et al. (1997), and the dashed line is the limiting EIT resolution, 3.8 Mm.

August 3, 2000

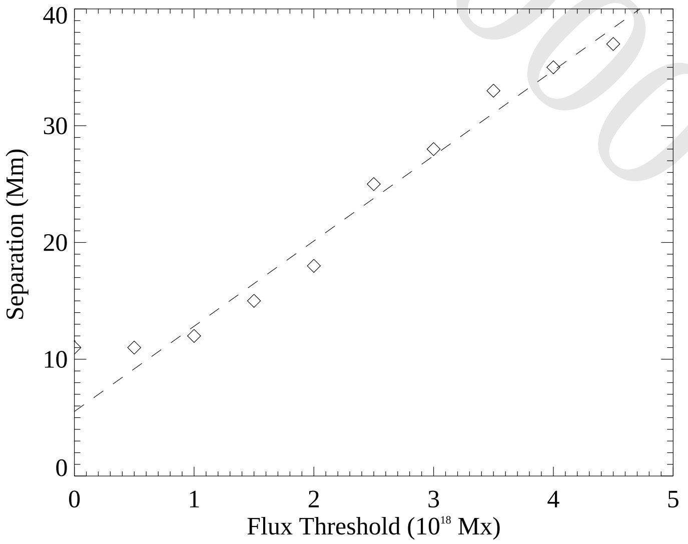

Fig. 8.— The relationship between threshold flux levels and separation between flux concentrations. MDI magnetograms were smoothed with a 1.2" Gaussian, then flux concentrations that were above the MDI two-sigma noise level (14 gauss) were counted. Flux concentrations greater than the threshold value were used to calculate the density of points and in turn the average cell diameter of the concentrations. The roll off below 1.5×10^{18} Mx is due to the selection process used in the flux concentration identification algorithm. Data courtesy H. J. Hagenaar.

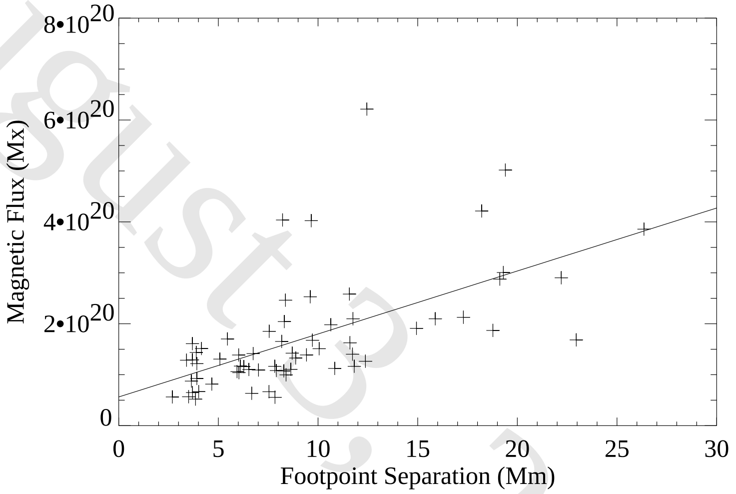

August 3, 2000

Fig. 9.— Footpoint separation versus total integrated unsigned magnetic flux. The footpoint separation was determined by the centroids of the magnetic flux concentrations, and the magnetic flux is the integral of the total flux defined by the projected area of the brightening in the Fe XII images and the loop footpoints.

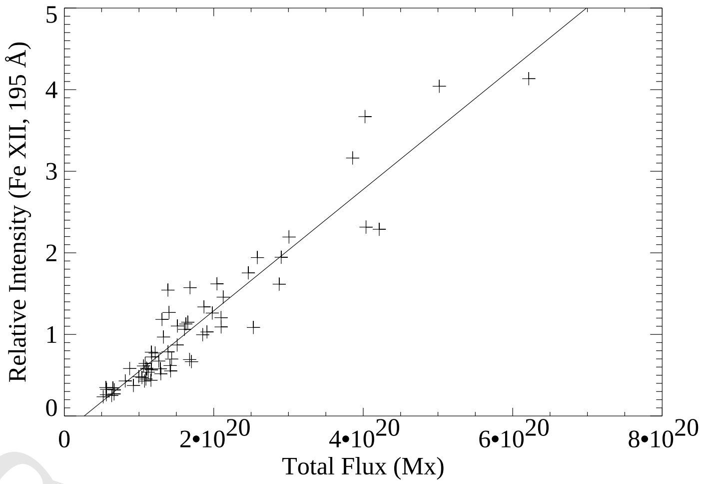

Fig. 10.— Relationship between integrated unsigned photospheric magnetic flux and total Fe XII loop intensity. The region of integration was chosen by selection a region surrounding the brightening visible in EIT and also including the footpoints as observed by MDI.

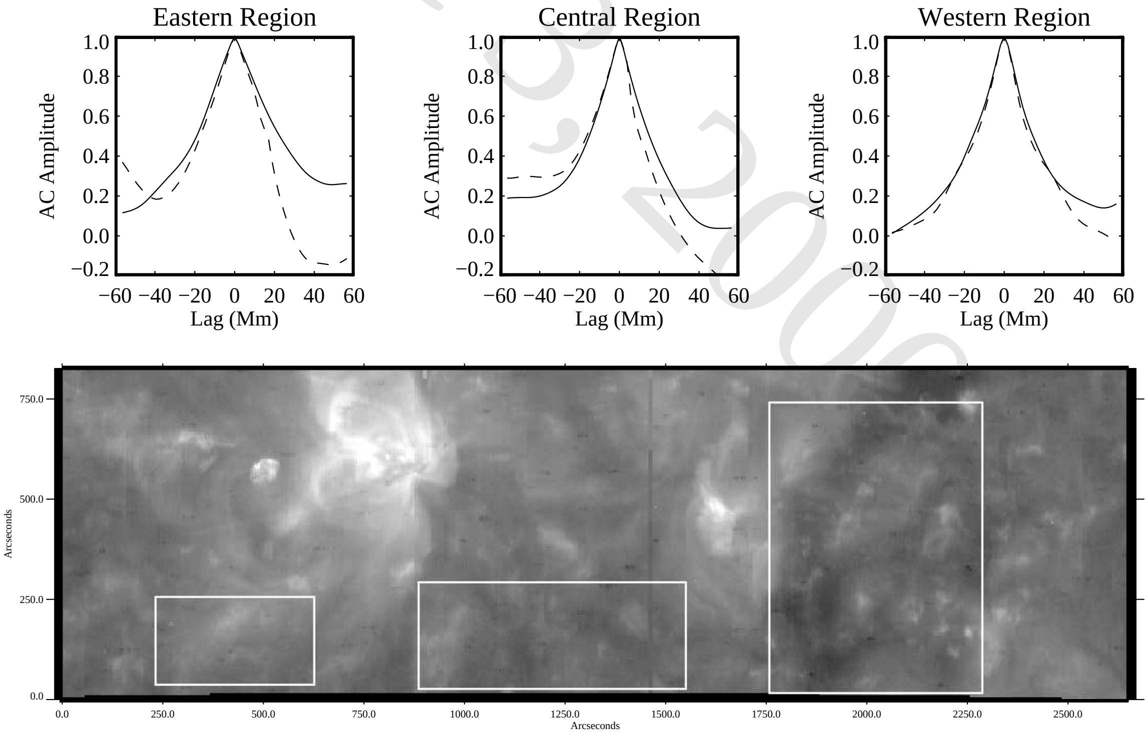

Fig. 11.— Averaged Fe XII autocorrelation curves. Solid lines are EW, dotted lines are NS.

The autocorrelation graphs correspond to the three quiet regions outlined in the lower figure. The eastern region is averaged over 47 frames, the central region over 100 and the western region over 51 frames. A distinct variation between EW and NS is seen in the eastern region (and to a lesser extent the central region), due to large loops from the active region passing over the field of view. The Western region is least affected by these overlying loops and the similarity in correlation distances suggests the orientation of quiet Sun brightenings is isotropic. The typical size scale (FWHM) is ≈ 26 Mm.

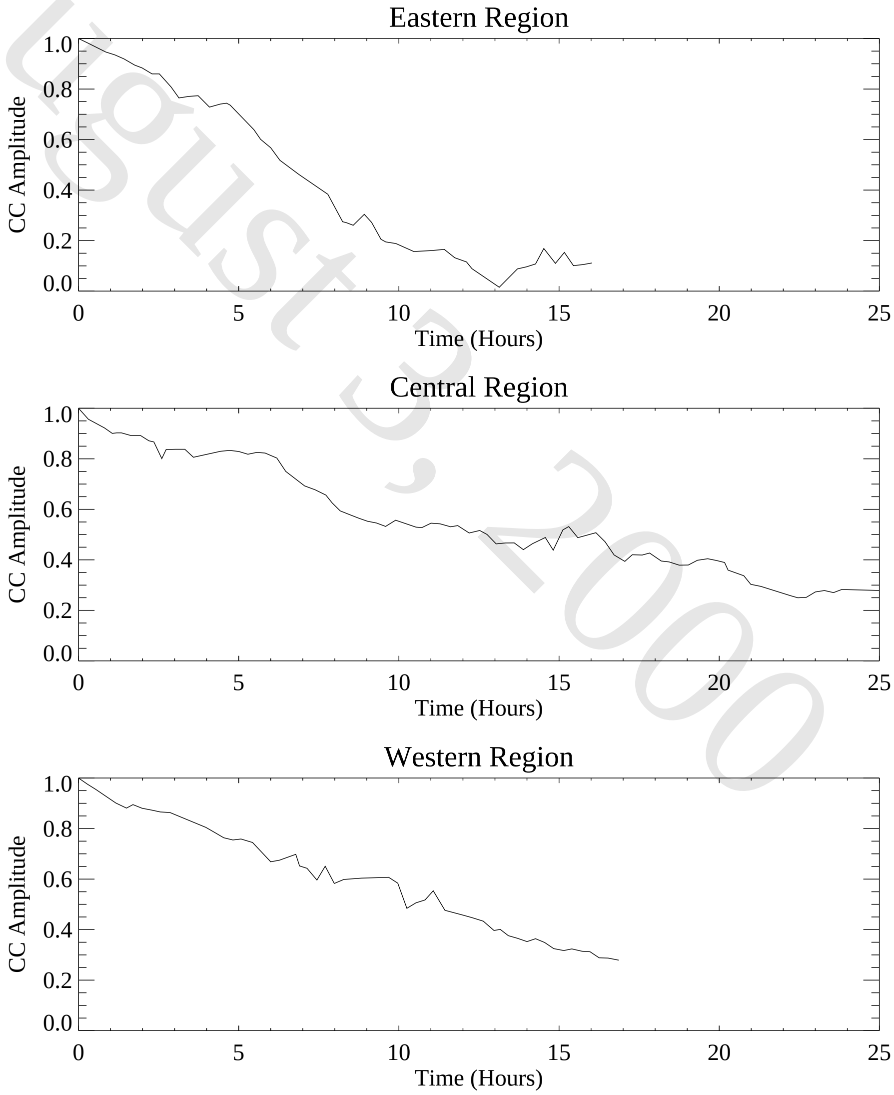

Fig. 12.— EIT/Fe XII cross-correlation in the quiet corona in the same regions as figure 11.

August 3, 2000

The top curve shows the greatest discrepancy in decorrelation bias due to the evolution of the large-scale loops emanating from the neighboring active region. The remaining two regions decorrelate in ≈ 12 hours.

August 3, 2000